Supporting Information File

for

Evaporation-Induced Formation of Blue-Emissive Guanine-Based Spherulitic Microstructures

Aditya Prasun, Ravindra Vishwakarma, Suryakamal Sarma, Tarun Kumar Sahu, Tridib K. Sarma*

Department of Chemistry, Indian Institute of Technology Indore, Simrol, Khandwa Road, Indore 453552, India

* Corresponding Author; Email- tridib@iiti.ac.in

1. Materials

Guanine, Sodium Hydroxide, Potassium Hydroxide were purchased from Merck, USA. Lithium Hydroxide Monohydrate was purchased from Otto Chemicals, India. All solutions were prepared using deionized water. All chemicals were used without any further purification.

2. Instrumentation

2.1 UV-visible spectroscopy

All UV–vis absorption spectra were recorded at room temperature (298 K) on an Agilent Cary 60 UV–vis spectrophotometer (Agilent Technologies, USA) equipped with a deuterium and tungsten-halogen lamp source and a photomultiplier tube detector. Measurements were carried out using a standard quartz cuvette of 1 cm path length (1 × 1 cm) with sample volume of 3.0 mL, and baseline correction was performed using DI water-filled cuvette under identical optical conditions.

2.2 Fluorescence spectroscopy

Steady-state emission and excitation spectra were recorded using a Fluoromax-4P spectrofluorometer (Horiba Jobin Yvon, model FM-100) equipped with a 150 W xenon lamp as the excitation source. Emission and excitation wavelengths were scanned over the range of 200–950 nm, using a fixed slit width of 2 nm × 2 nm for both the excitation and emission monochromators to ensure consistent spectral resolution across all samples. All spectra were corrected for the spectral sensitivity of the detection system using the instrument's built-in correction functions. Measurements were carried out at 298 K using a temperature-controlled cell holder to maintain constant experimental conditions.

Fluorescence analysis of the dried solid assemblies was performed using the Horiba solid-state sample holder, with a slit width of 5 nm × 5 nm.

2.3 Fourier Transform Infrared (FTIR) spectroscopy

Fourier-transform infrared (FTIR) spectra for all samples were recorded in powder form using a Bruker ALPHA II Platinum attenuated total reflectance (ATR) spectrometer equipped with a diamond-coated ZnSe crystal. Measurements were performed in the wavenumber range of 400–4000 cm^{-1}, with a spectral resolution of 4 cm^{-1} and 16 co-added scans per sample to enhance signal-to-noise ratio. Background spectra were acquired from the clean ATR crystal prior to each measurement, and sample powders were gently pressed onto the crystal surface to ensure uniform contact.

2.4 Field Emission Scanning Electron Microscopy (FESEM)

Field-emission scanning electron microscopy (FE-SEM) was performed using a Zeiss Gemini 360 field-emission scanning electron microscope (Carl Zeiss, Germany). A small volume (10 μL) of guanine solution was drop-cast onto a clean glass substrate, allowed to air-dry under ambient conditions to facilitate crystal formation, and subsequently coated with a 5 nm-thick layer of gold using a high-vacuum sputter to minimize charging effects and enhance secondary-electron emission. ImageJ (version 1.x, NIH, USA) was used for post-acquisition

processing and analysis of the SEM micrographs scale-bar addition, and particle-size measurements via manual or threshold-based segmentation. The processed SEM images were then pseudo-colored using GIMP (GNU Image Manipulation Program) to enhance visual contrast and highlight morphological features while preserving the original grayscale intensity information to avoid misleading interpretation.

2.5 Fluorescence Microscopy

Microscopic investigations of various guanine samples were carried out using an inverted Nikon Eclipse Ts2R-FL fluorescence microscope (Nikon Instruments, Japan), equipped with a DS-Fi3 color CMOS camera (5.9 MP, 2880 × 2048 pixels; USB 3.0 interface) and a high-intensity LED illumination system for both bright-field and epi-fluorescence imaging. Bright-field and phase-contrast imaging were performed using Plan Fluor air-immersion objectives of 10× (NA 0.25) and 20× (NA 0.40), while high-magnification detail was acquired using a 100× oil-immersion objective (NA 1.40). Fluorescence imaging was conducted with a four-channel LED-based epi-fluorescence system, employing standard filter cubes (e.g., DAPI, FITC, and Texas Red-type channels, 385–625 nm excitation range) to capture intrinsic fluorescence from dropcasted samples on a cover slip. Acquired images were processed, annotated, and analyzed using NIS-Elements Imaging Software (version D 5.20).

2.7 Time Correlated Single Photon Counting (TCSPC)

Fluorescence decay profiles of liquid samples were recorded on Horiba instrument (Fluorocube-01-NL) and 371 nm laser source was used for excitation. Curve fitting was performed on Data analysis software to get average lifetime values. . All decay curves were analyzed using dedicated data analysis software, employing a multiexponential fitting model:

$$\boldsymbol{I(t) = \sum \alpha_i \exp\left(-\frac{t}{\tau_i}\right)}$$

where τ_i and α_i represent the lifetime and amplitude of each component, respectively. The average lifetime ($\langle\tau\rangle$) was calculated as:

$$\boldsymbol{\langle \tau_i \rangle = \frac{\sum \alpha_i \tau_i}{\sum \alpha_i}}$$

Optimal fitting was achieved by maintaining the reduced chi-squared (χ^2) value close to unity for all measurements.

2.8 Quantum Yield Calculations

Absolute quantum yields of solid samples were measured using a Horiba QuantaMaster 8450-22 steady-state photoluminescence spectrophotometer equipped with an integrating sphere. For liquid samples, relative quantum yields were determined using quinine sulfate (quantum yield = 0.54 in 0.1 M H_2SO_4) as the reference standard, with excitation at 360 nm. The quantum yield (Φ_{sample}) was calculated using the following equation:

$$\phi_{sample} = \phi_{standard} \frac{F_{sample}}{F_{Standard}} \frac{f_{standard}}{f_{sample}} \left(\frac{\eta_{sample}}{\eta_{standard}}\right)^2$$

2.8 Powder X-Ray Diffraction (P-XRD)

Powder X-ray diffraction (PXRD) analysis was carried out on a Rigaku powder X-ray diffractometer (Rigaku Corporation, Japan), typically equipped with a Cu Kα radiation source (λ = 1.5406 Å) and a graphite monochromator, operating at a tube voltage of 40 kV and a tube current of 30–40 mA. The freshly prepared solution was dropcast on a precleaned glass substrate and was left to dry under controlled humidity conditions which was then used for recording the PXRD data.

2.9 pH measurement

The pH measurements were performed using a benchtop digital pH meter (LabMan Instruments Ltd., India) equipped with a combination glass electrode. The instrument was calibrated prior to use by a two-point calibration procedure employing standard buffer solutions of pH 4.0 and 7.0. All measurements were conducted at ambient laboratory temperature (298 K).

The pH of the 0.2 M NaOH solution was measured to be approximately 13.0, which is slightly lower than the theoretical value of 13.3. This deviation is likely attributable to the reduced accuracy of glass electrodes at high pH values and instrumental limitations under highly alkaline conditions. Therefore, the pH values reported in the manuscript correspond to the experimentally measured readings obtained from the pH meter and are not intended to represent exact theoretical values.

3. Methods

3.1 Solution Preparation

In a typical procedure, 25 mM guanine (Molecular Weight (MW) = 151.2 g/mol) was added to a 0.2 M aqueous solution of NaOH (MW = 40 g/mol). The resulting solution was further subjected to ultrasonication to ensure complete solubilization verified by resulting transparent solution. Further various solutions were prepared by varying guanine and base concentration to observe their effect on its photophysical or morphological behaviour. Freshly prepared solutions were drop-cast onto pre-cleaned glass coverslips (or glass slides for SEM and PXRD measurements). Prior to use, the substrates were sonicated in chromic acid cleaning solution to remove organic contaminants, thoroughly rinsed with soap water followed by deionized water, and subsequently dried under ambient conditions before sample deposition.

For observing the effect of alkali metal cation, all other conditions were kept unchanged except for the base ($LiOH.H_2O$ and KOH).

3.2 Microscopic Analysis

Unless otherwise specified, 10 μL of guanine solution was drop-cast onto a glass coverslip and allowed to dry under ambient conditions. For in situ microscopic

investigations, the solution was drop-cast directly onto coverslips mounted on the microscope stage, and imaging was initiated immediately.

3.3 Relative Humidity Experiments

To observe the effect of humidity, 10 μL of guanine solution was dropcasted on a glass cover-slip. The coverslip was then immediately kept in a preadjusted environmental chamber for desired humidity level while keeping the temperature constant (298 K) for all the sets. For each experiment at least 3 sets were analyzed.

3.4 Average diameter and Circularity calculations

The recorded micrographs of the spherulitic structures were analyzed using NIS-Elements software (Nikon, Japan) and/or ImageJ software (NIH, USA) for quantitative morphological analysis. The size distribution and circularity of the structures were determined from multiple representative micrographs acquired under identical imaging conditions. Prior to analysis, the images were calibrated using the microscope scale bar.

The circularity of the structures was calculated using the following relation:

$$\boldsymbol{Circularity = 4\pi A/P^2}$$

Where A and P represent area and perimeter, respectively. A circularity value of 1.0 corresponds to a perfect circle, while lower values indicate increasing deviation from circular geometry.

3.5 Fractal Dimension Analysis

Fractal dimension analysis was performed using the box-counting method implemented in ImageJ software (NIH, USA). Optical/SEM images of the assemblies were first converted to 8-bit grayscale and threshold to obtain binary images. The fractal dimension (D_f) was then calculated using the FracLac/ImageJ box-counting algorithm by analyzing the scaling relationship between the number of occupied boxes and the box size over an appropriate range of scales. The fractal dimension was obtained from the slope of the linear fit in the log(N) versus log(1/ε) plot, where N is the number of occupied boxes and ε is the box size. Multiple representative structures were analyzed to ensure reproducibility before the average fractal dimension values were reported.

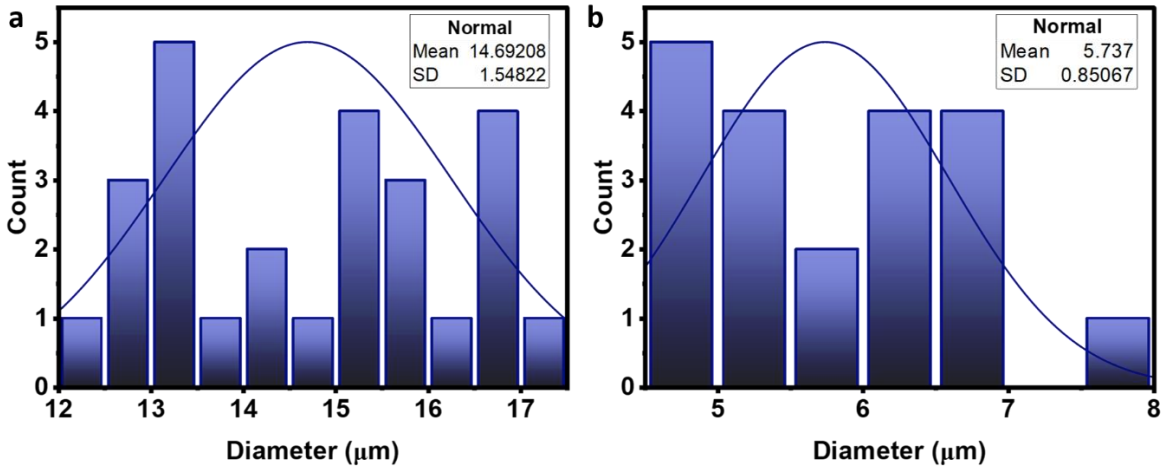

Figure S1. Average diameter of spherulites formed (a) larger spheruliltes (b) smaller spherical assemblies as observe in the optical microscope.

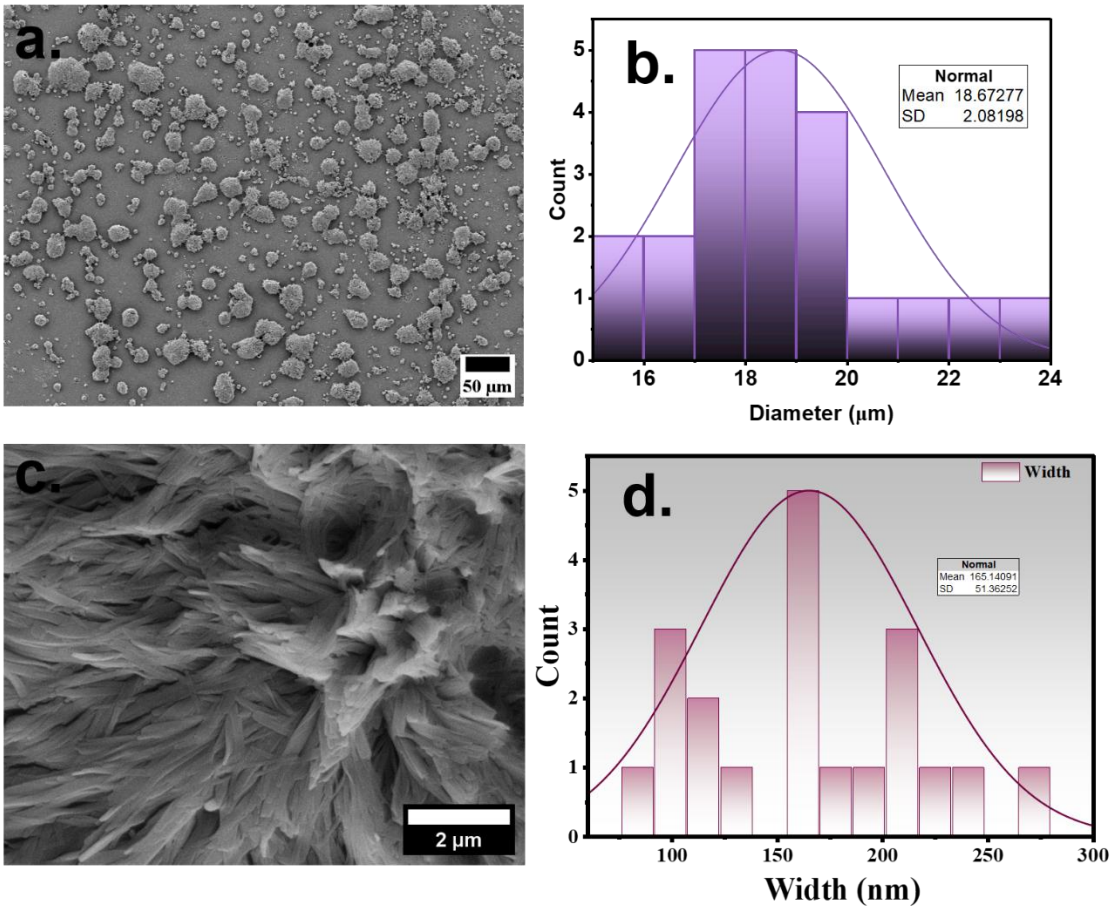

Figure S2. SEM micrograph (a,c) and corresponding diameter distribution curve (b,d) for spherulitic aggregates at lower (a) and higher (c) magnification.

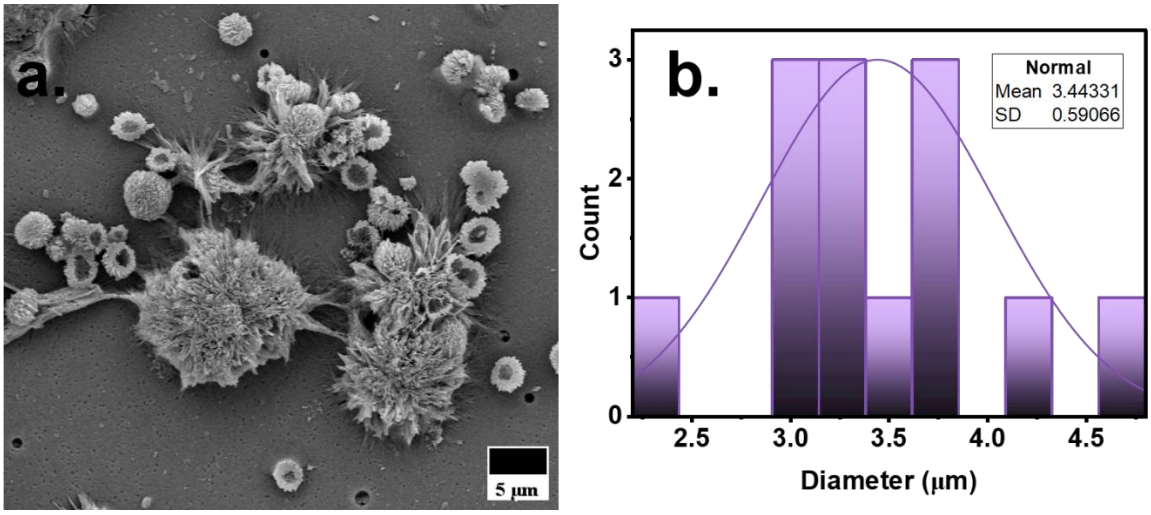

Figure S3. SEM image (a) and corresponding size distribution curve for smaller spherical assemblies observed.

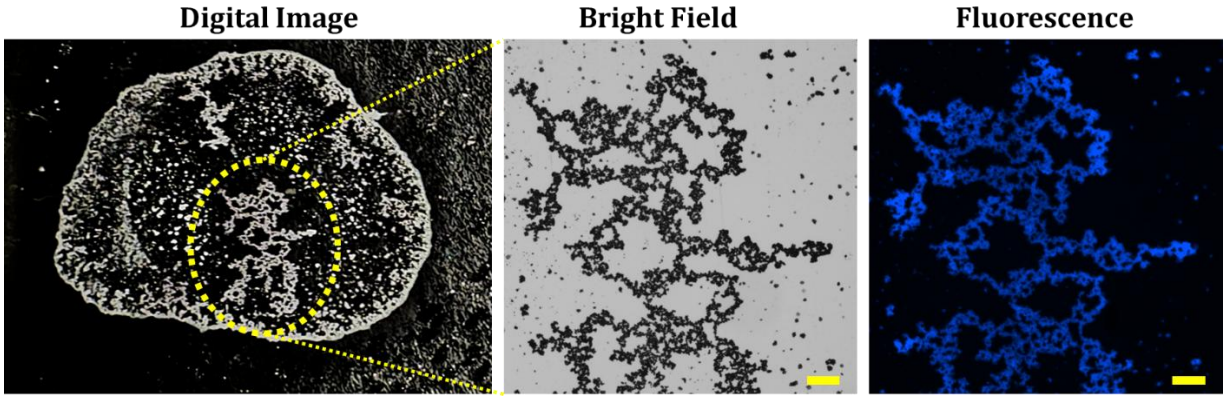

Figure S4. (a) Digital image of the dried drop-cast region displaying a fractal arrangement of aggregated spherulites. (b) Bright-field and (c) fluorescence micrographs of the corresponding fractal architecture, highlighting its structural organization and intrinsic emission. (Scale bar: 200 µm).

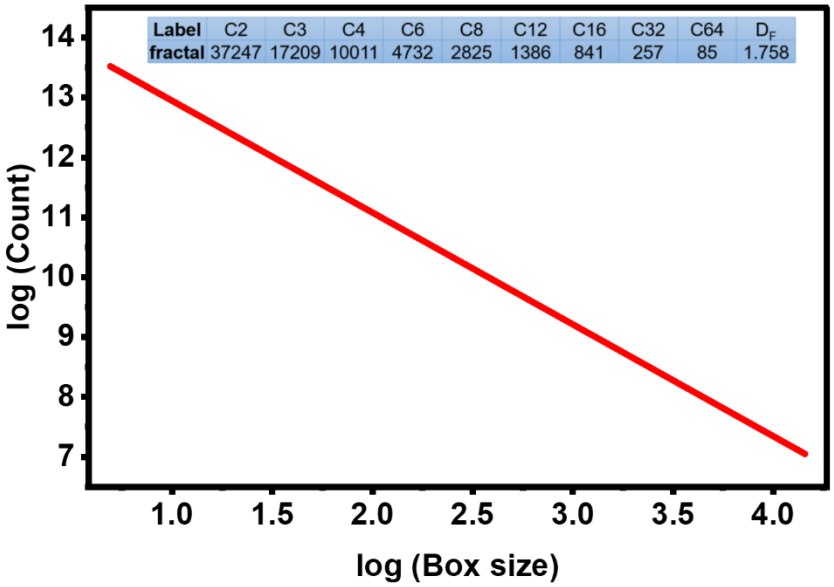

Figure S5. Graph between log(count) vs log (box size) using which fractal dimension were calculated.

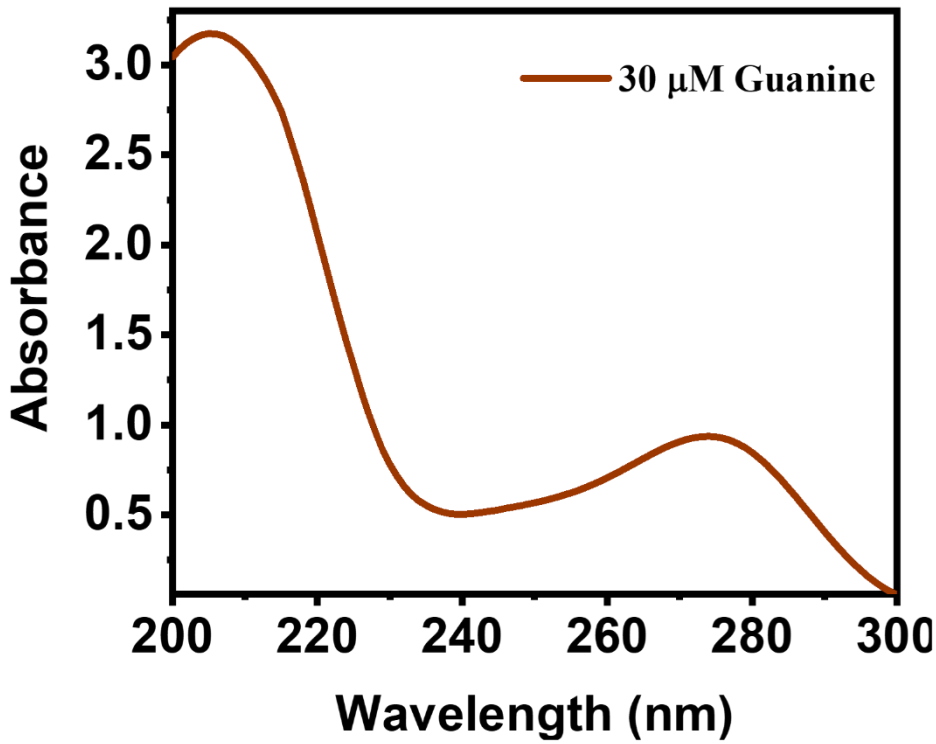

Figure S6. UV-visible spectrum of guanine dissolved in 0.2 M aqueous solution of NaOH showing characteristic peaks of guanine dianion.

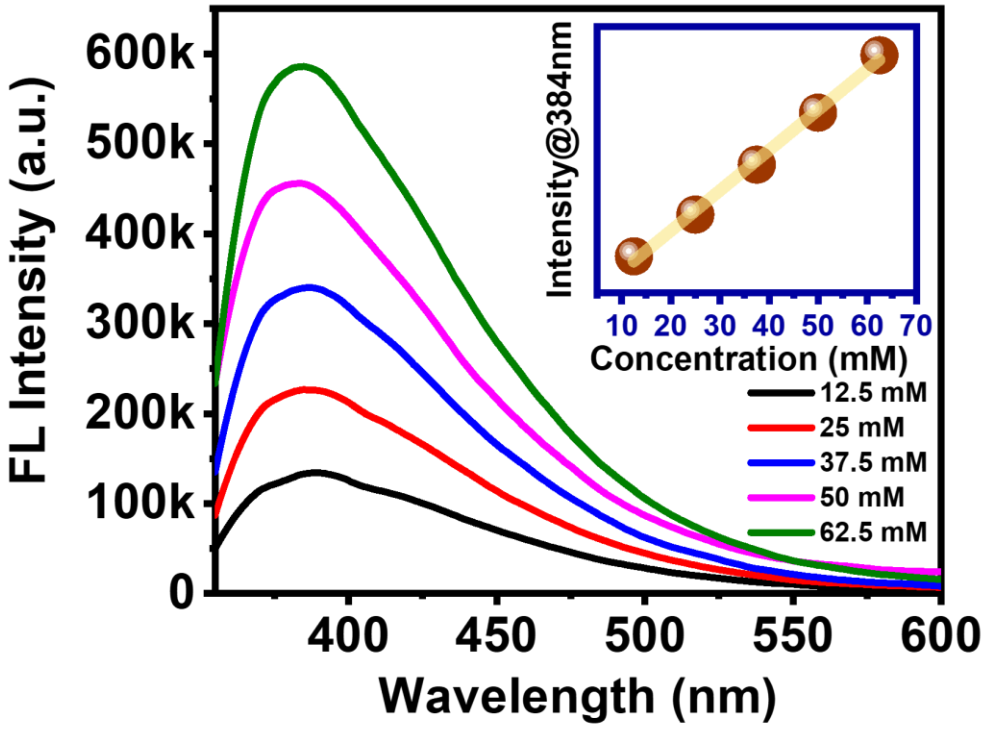

Figure S7. Concentration dependent emission spectra of guanine (12.5-67.5 mM) dissolved in 0.2 M NaOH solution

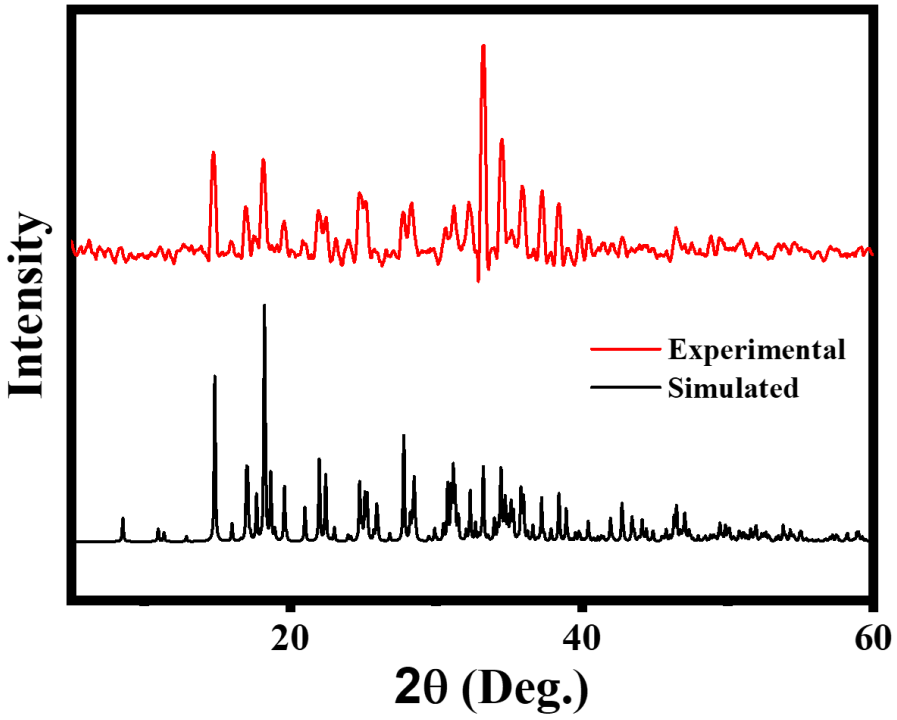

Figure S8. PXRD pattern of dried 0.2 M NaOH solution showing resemblance with the simulated pattern of disodium guanine heptahydrate.

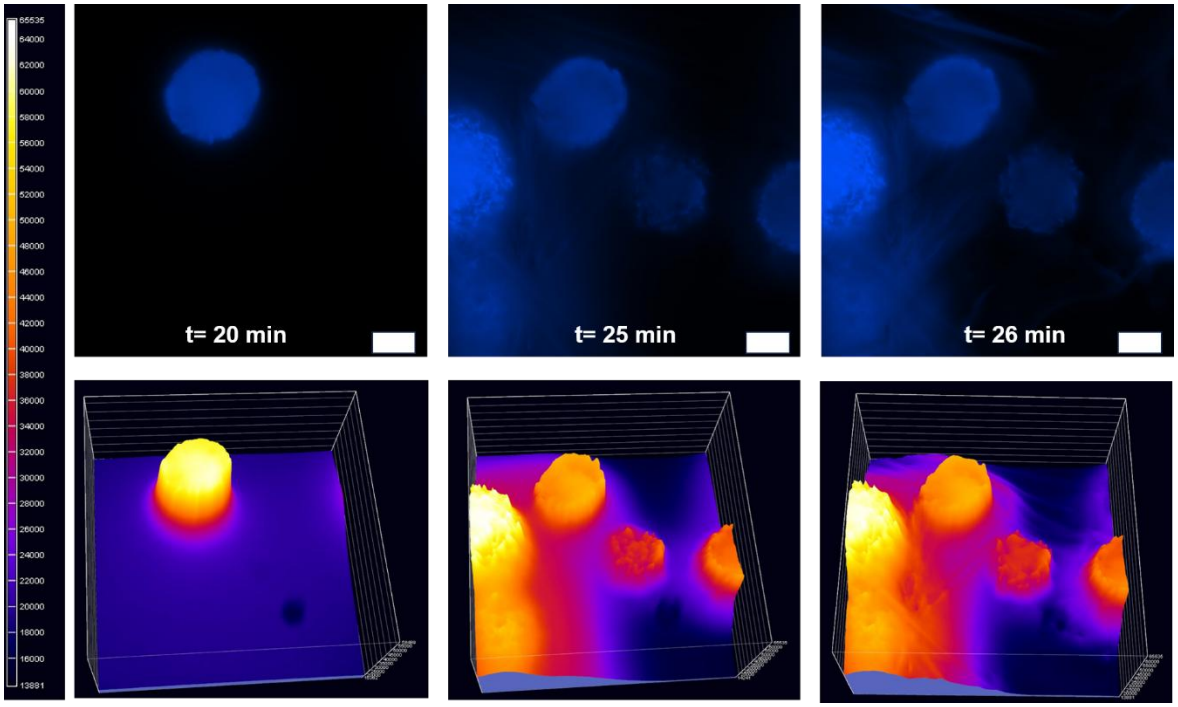

Figure S9. Snapshots and corresponding intensity surface plots showing evolution of fibrous architectures at the final stage of evaporation which shows significantly lower emission in comparison to the spherical assemblies. (scalebar: 10 μm)

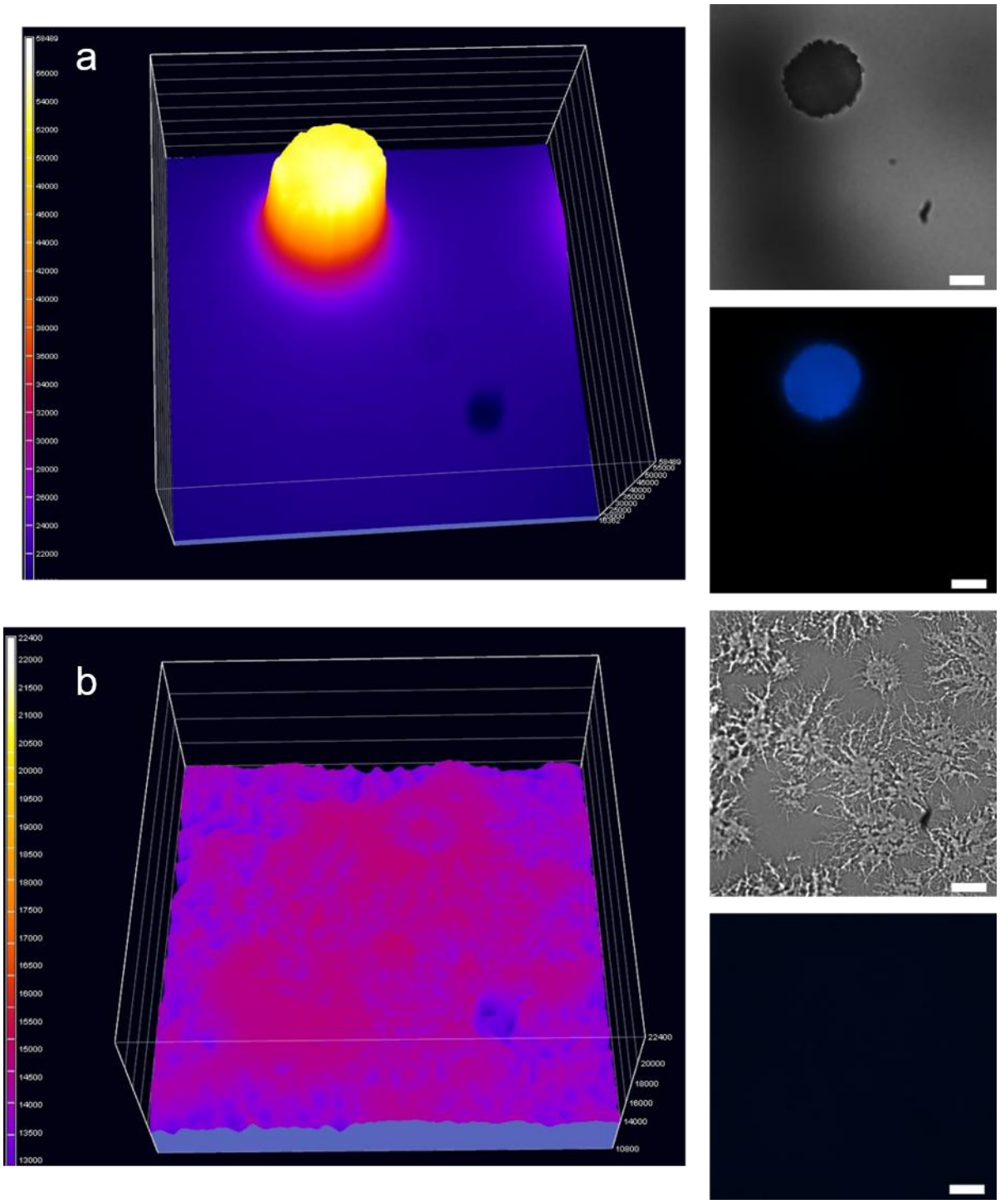

Figure S10. Intensity surface plots for corresponding brightfield and fluorescence images of spherulites (a) and fibres (b) formed at higher and lower humidity levels respectively.

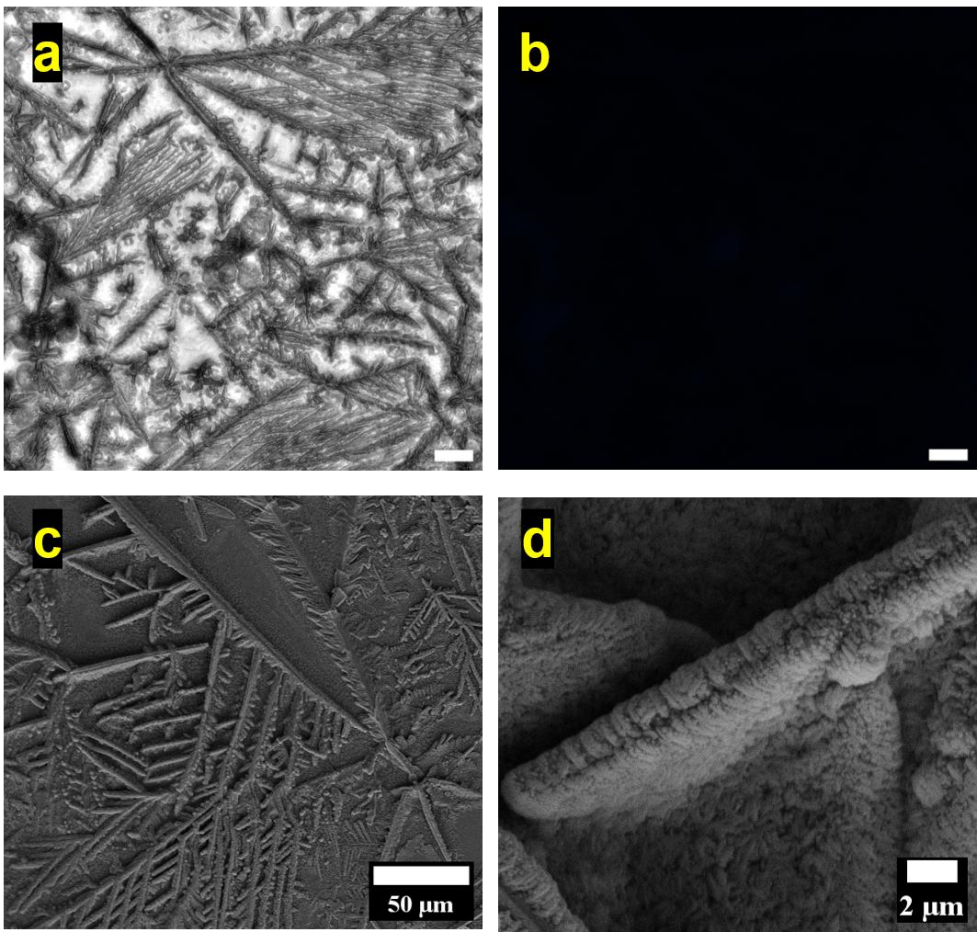

Figure S11. Effect of temperature on the self-assembly of guanine leading to Dendritic structures formed at elevated temperatures; brightfield (scalebar: 20 µm) (a), fluorescence (b), and SEM micrographs at lower (c) and higher (d) magnification.

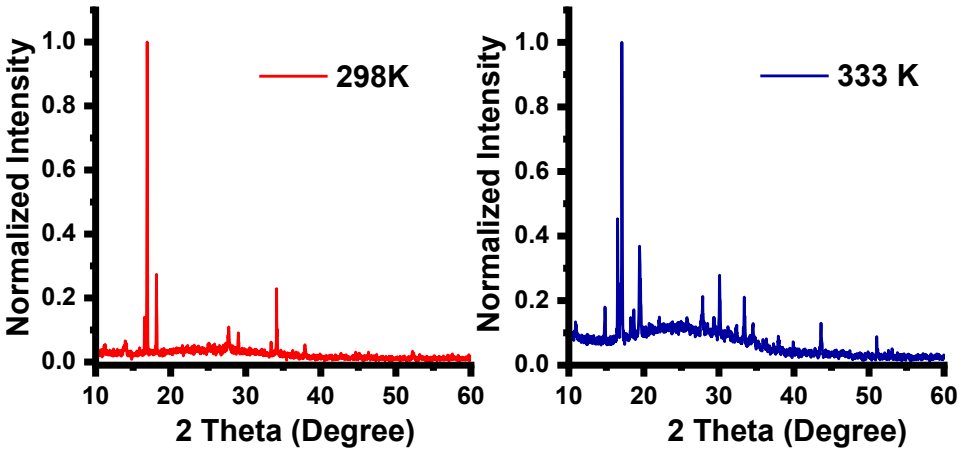

Figure S12 PXRD pattern of guanine assemblies at 298 K and 323 K. At higher temperature of self-assembly, broad hump observed supports formation of amorphous assembly owing to faster evaporation.

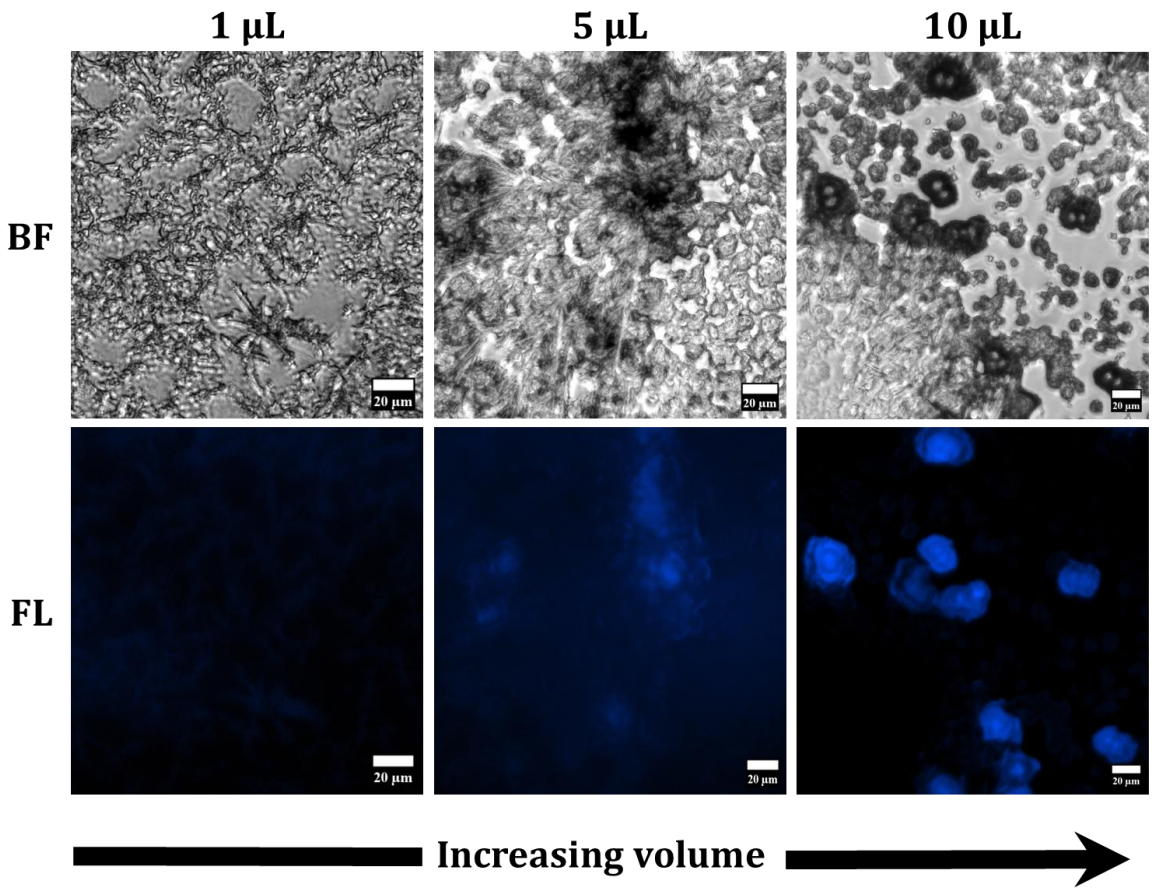

Figure S13. Effect of drop-cast solution volume on the morphology of guanine assemblies formed on glass coverslips. Lower solution volumes lead to rapid solvent evaporation, resulting in the formation of fractal architectures. In contrast, larger volumes promote slower evaporation, yielding well-defined spherulitic structures.

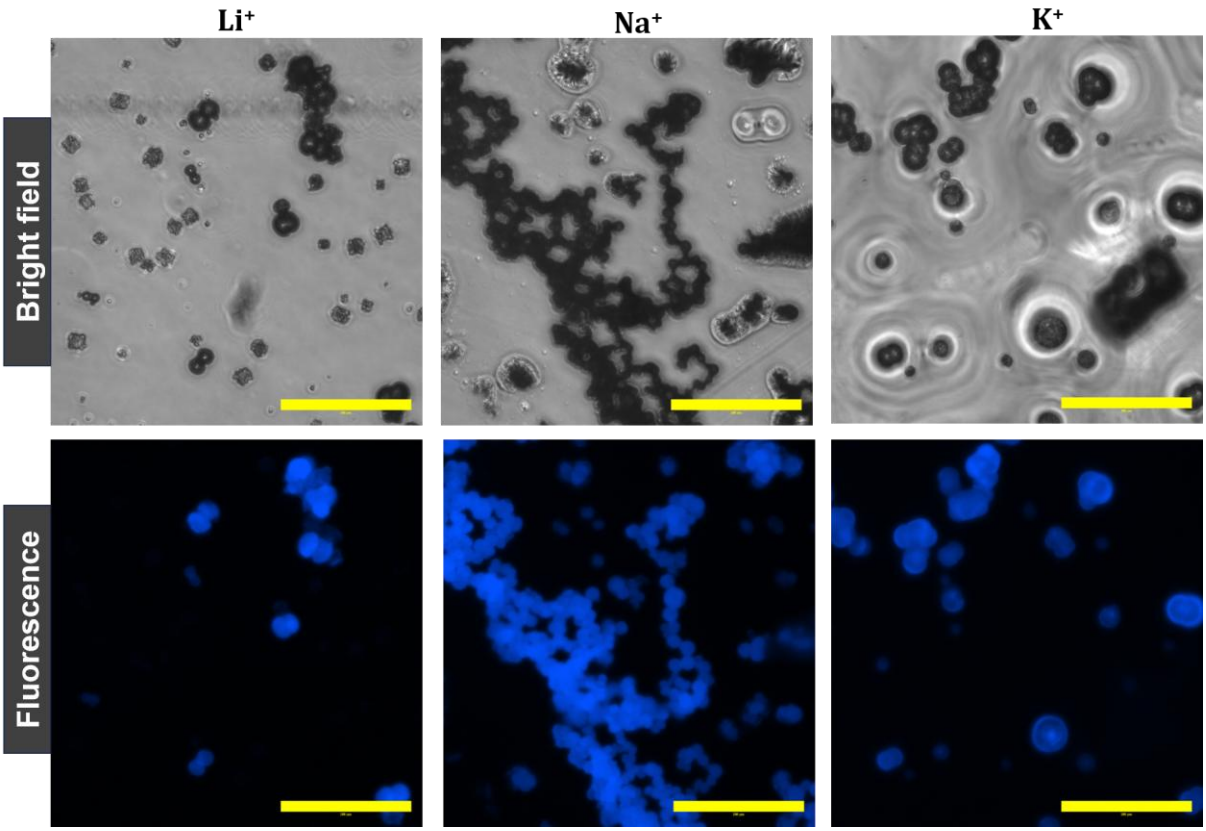

Figure S14. Bright field and fluorescence microscopic images confirm formation of blue emissive spherulitic architectures in the presence of different alkali metal cation.

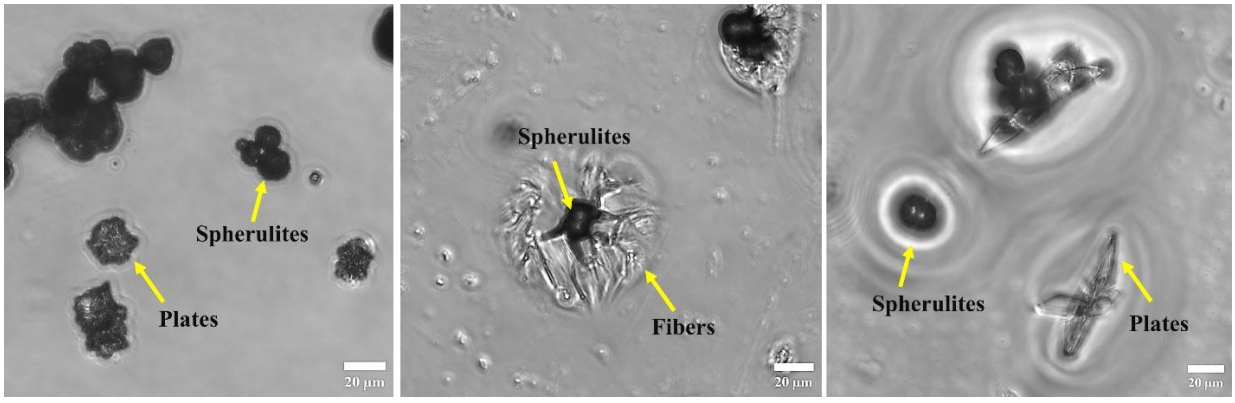

Figure S15. Optical micrographs showing formation of spherulites in all three basic medium along with other morphologies such as radially arranged plates in LiOH, fibres in NaOH and plates in KOH

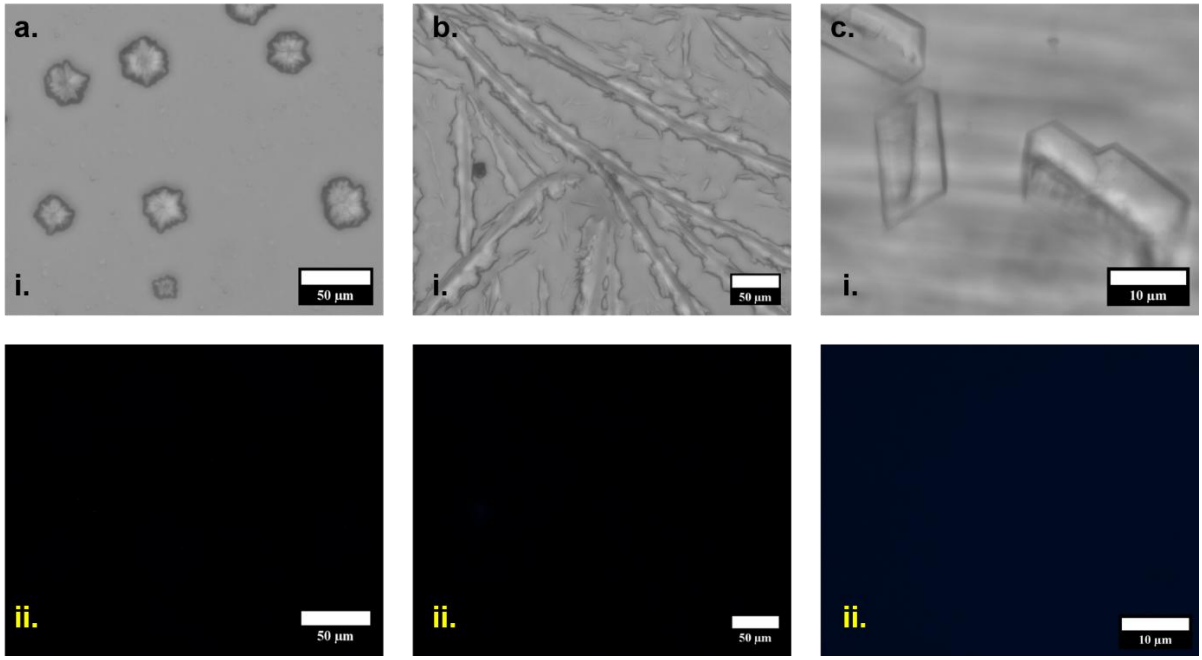

Figure S16. Brightfield (i) and fluorescence (ii) microscopic images of architectures evolved post evaporation of water from 0.2 M solution of (a) $LiOH{\cdot}H_2O$, (b) NaOH, and (c) KOH in absence of guanine.

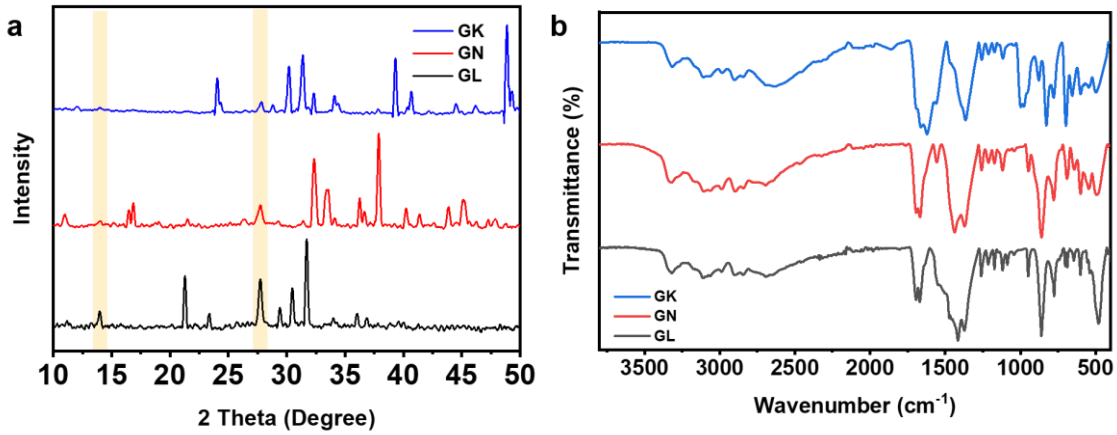

Figure S17. Comparison of (a) PXRD pattern and (b) FTIR spectra of spherulitic assemblies of guanine formed under different alkali metal bases (0.2 M). Highlighted peaks in the PXRD pattern, common to all samples, correspond to π–π stacked guanine layers, while other sharp peaks match well with the signature peaks of the respective bases. FTIR spectra show similar features across all samples, confirming the presence of a common guanine moiety.

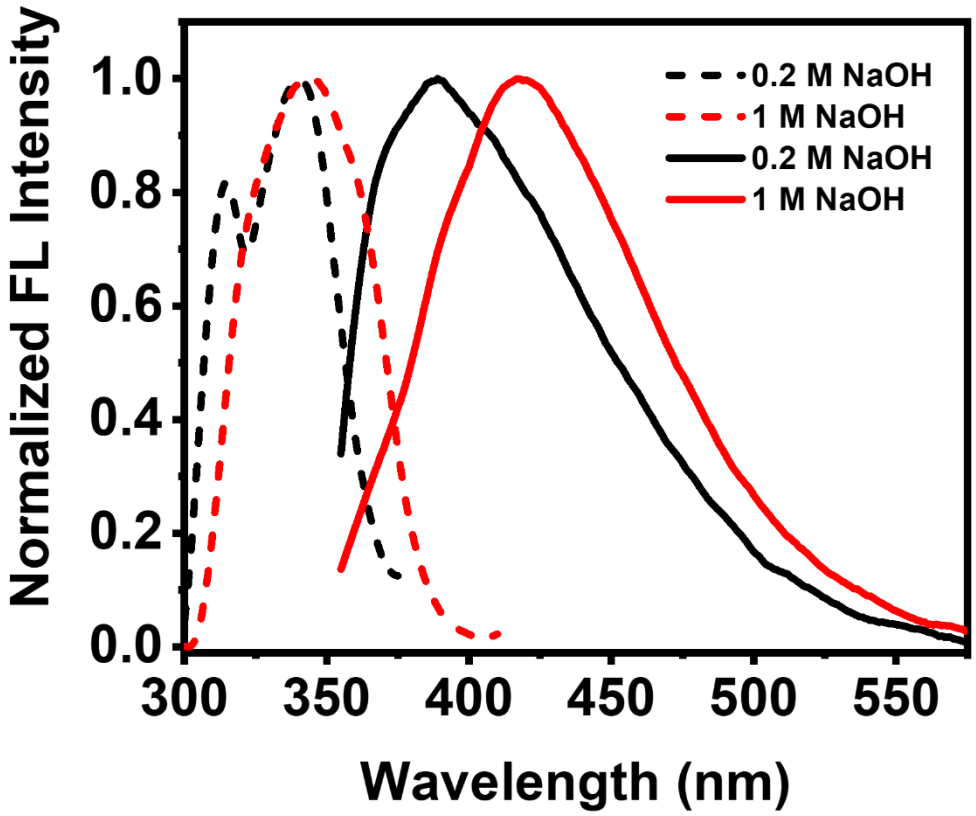

Figure S18. Effect of NaOH concentration on emissive behaviour of guanine.

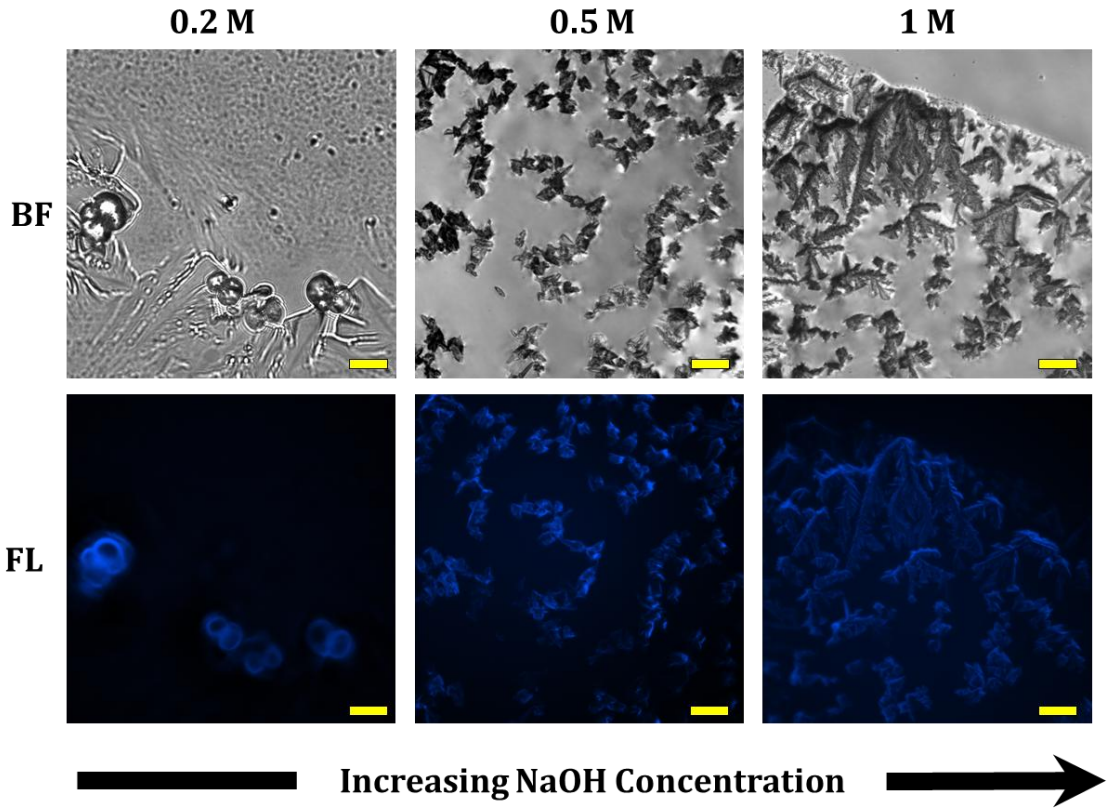

Figure S19. Effect of NaOH concentration on the morphology of guanine assemblies (scale bar: 100 μm). At lower NaOH concentrations, well-defined spherulitic structures are predominantly observed. At intermediate concentration (0.5 M), irregularly shaped microcrystals become dominant, whereas higher concentrations promote the formation of branched, dendritic architectures. These observations indicate that lower base concentrations favor spherulitic assembly, while increasing alkalinity drives non-equilibrium growth pathways.

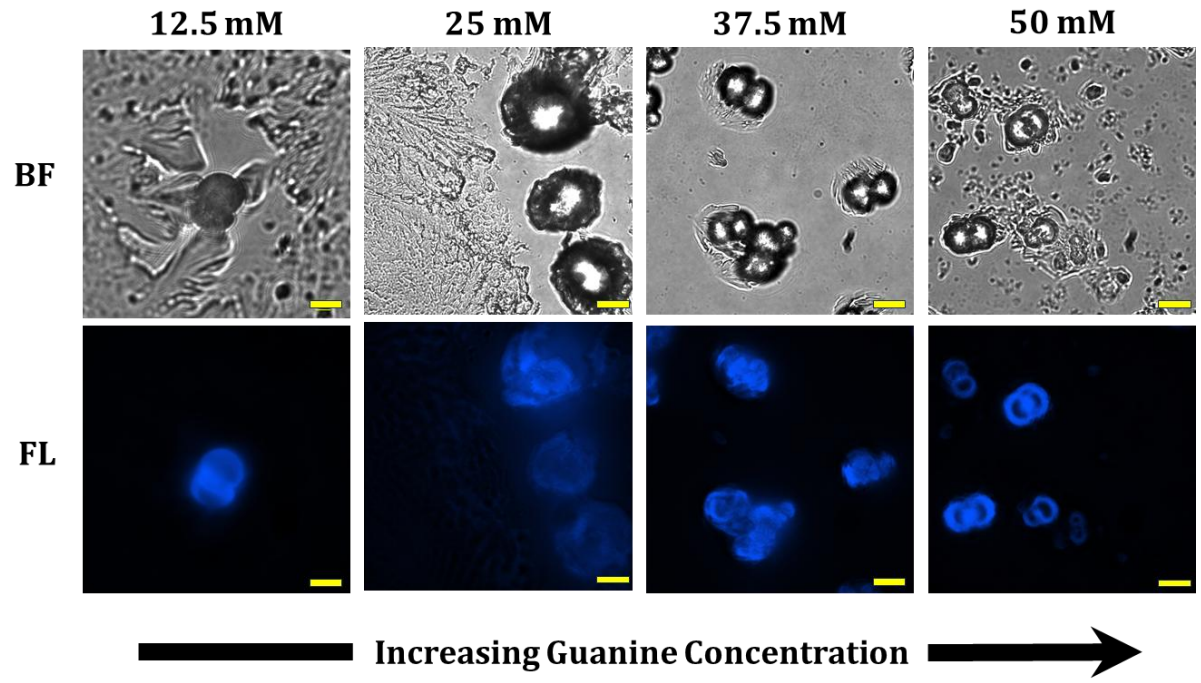

Figure S20. Effect of guanine concentration on self-assembly at a constant NaOH concentration (0.2 M). Across the examined concentration range, well-defined spherulitic structures are consistently formed, indicating that guanine concentration has minimal influence on morphology under fixed alkalinity, primarily affecting the size and packing density of the assemblies. (Scale bar: 20 μm)

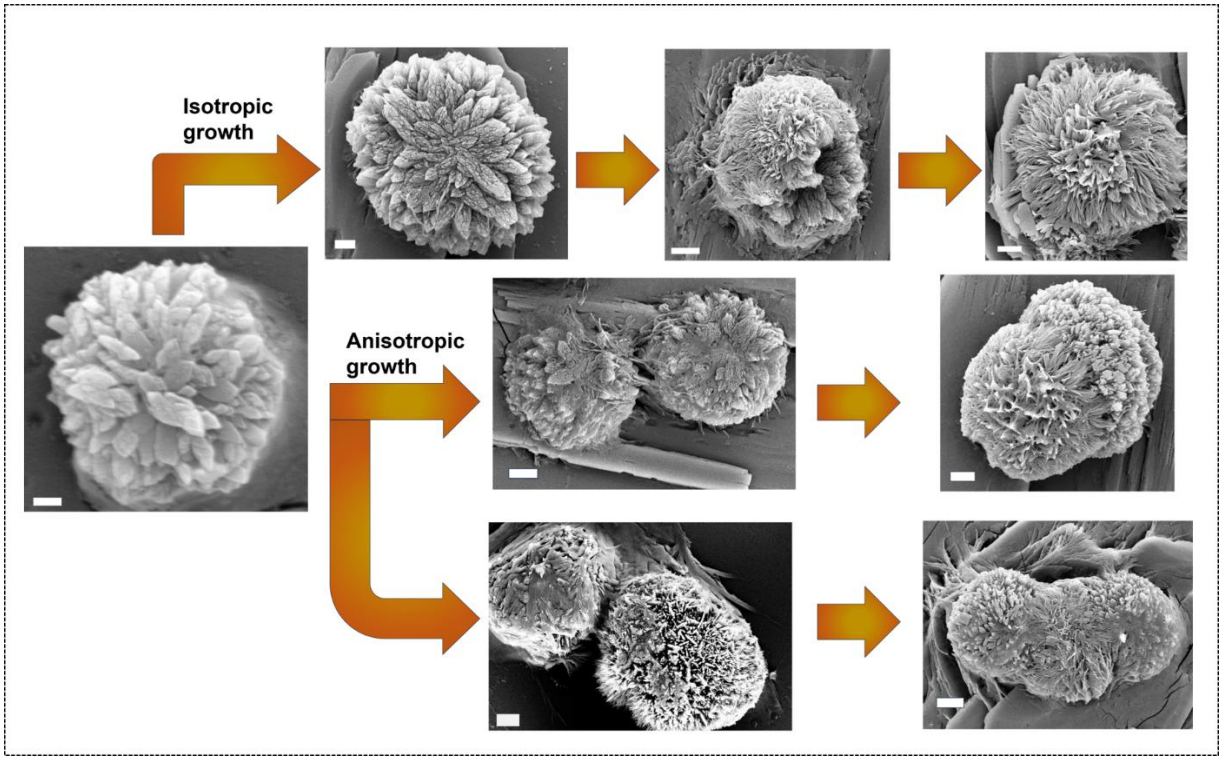

Figure S21. Microscopic evidences suggest the spherulite formation proceeds via both isotropic and anisotropic growth pathways.